PCCP

ROYAL SOCIETY OF CHEMISTRY

PAPER

View Article Online
View Journal | View Issue

Cite this: *Phys. Chem. Chem. Phys.*, 2023, **25**, 9626

Study of pnictides for photovoltaic applications†

Jayant Kumar and Gopalakrishnan Sai Gautam *

Received 24th September 2022,
Accepted 7th March 2023

DOI: 10.1039/d2cp04453f

rsc.li/pccp

For the transition into a sustainable mode of energy usage, it is important to develop photovoltaic materials that exhibit better solar-to-electricity conversion efficiencies, a direct optimal band gap, and are made of non-toxic, earth abundant elements compared to the state-of-the-art silicon photovoltaics. Here, we explore the non-redox-active pnictide chemical space, including binary A_3B_2, ternary AA'_2B_2, and quaternary $AA'A''B_2$ compounds (A, A′, A″ = Ca, Sr, or Zn; B = N or P), as candidate beyond-Si photovoltaics using density functional theory calculations. Specifically, we evaluate the ground state configurations, band gaps, and 0 K thermodynamic stability for all 20 pnictide compositions considered, besides computing the formation energy of cation vacancies, anion vacancies, and cation anti-sites in a subset of candidate compounds. Importantly, we identify $SrZn_2N_2$, $SrZn_2P_2$, and $CaZn_2P_2$ to be promising candidates, exhibiting optimal (1.1–1.5 eV) hybrid-functional-calculated band gaps, stability at 0 K, and high resistance to point defects (formation energies >1 eV), while other possible candidates include $ZnCa_2N_2$ and $ZnSr_2N_2$, which may be susceptible to N-vacancy formation. We hope that our study will contribute to the practical development of pnictide semiconductors as beyond-silicon light absorbers.

1 Introduction

The 21st century world is in need of a dramatic shift in the energy sector, given the increasingly unsustainable nature of fossil fuel usage and the associated climate change. Among renewable sources, solar energy, *i.e.*, the conversion of solar radiation into electricity *via* photovoltaics (PVs), has significant potential in reducing our fossil fuel usage.[1] Notably, the Shockley–Queisser limit for maximum efficiency in single-junction PV devices requires semiconductors with a direct band gap in the 1.1–1.5 eV range.[2] Commercially, PVs are typically made based on crystalline Si, and do require larger material quantities (*i.e.*, PV panels are thick) and higher manufacturing hosts, necessitated by the indirect band gap (1.12 eV) of Si.[3] Thus, engineering and discovering direct gap semiconductors, which exhibit a 1.1–1.5 eV band gap, are made out of environmentally sustainable and non-toxic elements, and are reasonably cheap to manufacture, is still an active area of research.[4–6]

Semiconductors that have been explored as potential beyond-Si photovoltaics, which are often compounds, include (In,Ga)As, CdTe, Cu_2ZnSnS_4 (CZTS), $Cu_2InGaSe_4$ (CIGS), and their doped counterparts. There are several challenges in utilizing the aforementioned compounds as PVs, including some of the elements being toxic (*e.g.*, As in (In,Ga)As), lack of abundance of elements (*e.g.*, Te in CdTe[7]), difficulties in synthesis of phase-pure compounds resulting in the presence of secondary phases (*e.g.*, secondary phases of Cu–Se and Ag–Cu–Se forms in (Ag,Cu),(In,Ga)Se_2[8]) and the spontaneous formation of detrimental point defects (*e.g.*, Cu_{Zn} + Zn_{Cu} and Sn_{Zn} + $2Cu_{Zn}$ anti-site clusters in CZTS). In particular, point defects that form either during synthesis or processing (*e.g.*, high temperature annealing) can be harmful in reducing PV performance, by introducing structural distortions, altering the band gap, and/or formation of deep trap states within the band gap. Hence, it is important to evaluate the tendency to form intrinsic point defects while considering any novel semiconductor compound as a PV candidate.

Here, we explore a set of 20 pnictide compounds, including binary, ternary, and quaternary nitrides and phosphides, as potential PV candidates, using density functional theory (DFT[9,10]) calculations. Specifically, we explore pnictides of the formula, A_3B_2, AA'_2B_2, and $AA'A''B_2$ where A, A′ and A″ are permutations of different divalent cations and B is either N^{3-} or P^{3-}. We chose the chemical space of the above mentioned pnictides, partly inspired by the works of Kikuchi *et al.*[11] and Hinuma *et al.*,[12] with the constraint of choosing elements that are reasonably abundant and non-toxic to humans. Given the general chemical formula of A_3B_2, charge neutrality constraints and computational costs, we considered the combinations of

Department of Materials Engineering, Indian Institute of Science, Bengaluru 560012, India. E-mail: saigautamg@iisc.ac.in

† Electronic supplementary information (ESI) available: PAW potentials used, SCAN and HSE06 calculated DOS data, range of chemical potentials used for defect calculations, results from phonon calculations, and structural information on all theoretical structures considered. See DOI: https://doi.org/10.1039/d2cp04453f

several divalent cations in our compositions. Possible divalent cations that can constitute an A_3B_2 pnictide include alkaline earths (Mg, Ca, Sr, and Ba), and transition metals (V, Nb, Mn, Fe, Co, Ni, and Zn). We did not consider transition metals, except Zn, since they are redox-active and can result in recombination centers or carrier traps. We found Mg- and Ba-based nitrides to exhibit band gaps that are higher than the optimal range for photovoltaic applications. For example, $CaMg_2N_2$ exhibits 3.3 eV,[11] and $Ca(Mg_{1-x}Zn_x)_2N_2$ can have a band gap in the range of $\sim$3.3–1.9 eV depending on x,[13] while $BaMg_2N_2$ and $BaMg_2P_2$ have gaps of 2.49 eV and 1.80 eV, respectively.[14] Thus, we end up with pnictides, where possible cations are Ca, Sr, and Zn. Importantly, our choice of the pnictide chemical space has been explored by a few existing studies as possible PVs, such as Ca_3N_2, Zn_3N_2, Zn_3P_2, and $CaZn_2N_2$,[12,15–18] while a widespread theoretical or experimental screening for PV candidates has not been done so far.[19] We do note that our sampling of pnictides is only a subset of the possible compounds that can exist in nature.[20]

Apart from determining the ground state atomic configuration in disordered compounds, we evaluate their suitability as a PV material by calculating their band gap, 0 K thermodynamic and dynamic stability, and the formation energies of select point defects. Importantly, we identify five potential candidates, namely, $ZnCa_2N_2$, $SrZn_2N_2$, $ZnSr_2N_2$, $CaZn_2P_2$, and $SrZn_2P_2$, which exhibit an optimal (1.1–1.5 eV) band gap and are thermodynamically stable. Among the candidates that we have identified, $CaZn_2N_2$ and $SrZn_2N_2$ have been experimentally reported to exhibit band gaps of 1.90 eV and 1.60 eV, respectively.[11,12] Notably, considering point defect formation energies, we find $SrZn_2N_2$, $CaZn_2P_2$, and $SrZn_2P_2$ to be particularly promising since they exhibit a formation energy of >1 eV for cation vacancies, anion vacancies, and cation anti-sites. We hope that our study will reinvigorate research in the pnictide chemical space for potential PV materials, and will aid in the development of high efficiency, beyond-Si PVs that consist of sustainable and non-toxic constituents.

2 Methods

We calculated the total energies and electronic structures, for all pnictides considered, using DFT as implemented in the Vienna *ab initio* simulation package[21,22] and employing the projector-augmented-wave theory[23] (list of potentials used is provided in the ESI†). We used an energy cut-off of 520 eV on a plane-wave basis for all calculations, after validating the convergence of DFT-calculated total energy with various cut-off energies as shown in Fig. S1 of ESI.† We sampled the irreducible Brillouin zone using Γ-centred Monkhorst–Pack[24] meshes with a density of 32 k-points per Å, and used a Gaussian smearing with a width of 0.05 eV. We relaxed all structures by allowing the cell shape, cell volume, and ionic positions to change, without preserving symmetry, until the atomic forces and total energies reduced below $|0.01|$ eV Å^{-1}, and 10^{-5} eV, respectively, with the stress below a threshold of 0.2 GPa. Although we did not impose any symmetry constraints during our structural relaxation, particularly for the theoretically derived structures, we find the likelihood of the structural relaxation resulting in a structure that has a completely different symmetry from the initial configuration to be highly unlikely, since the theoretical structures were generated by chemical substitution at the uniquely defined symmetric sites.

We treated the electronic exchange–correlation interactions with the strongly constrained and appropriately normed (SCAN[25]) functional for all structure relaxation calculations. For the electronic density of states (DOS) calculations, we considered the converged ground state structure for each composition, and used the "fake" self-consistent field (SCF) procedure, with a mesh density of 64 k-points per Å. Note that the set of k-points sampled during the structure relaxation were retained with their original weights, while the newly introduced k-points were sampled with zero weights within the fake-SCF procedure. Since SCAN typically underestimates the band gap of semiconducting systems,[3,26–30] we also performed DOS calculations using the Heyd–Scuseria–Ernzerhof (HSE06[31]) hybrid functional, using an identical fake-SCF procedure and the SCAN-relaxed structures. For a select set of candidate pnictides, we calculated band structures using SCAN and the Setyawan–Curtarolo scheme to generate the list of symmetrically important k-points, as implemented in pymatgen.[32,33]

The initial crystal structure for a subset of the compounds considered in this work (see Table 1), were obtained from the inorganic crystal structure database (ICSD).[34] The calculated

Table 1 Details of structures obtained from ICSD, with their corresponding space groups. O and D indicate ordered and disordered structures, respectively. The number of unique orderings obtained upon enumeration are listed for disordered structures. The Wyckoff positions of unique cation sites are displayed in the final column on the right. The "*" in the space group column indicate the structures that were used as templates for generating other ternary, and quaternary compositions

Compounds	Space group	Ordered/dis-ordered (from ICSD)	Cations/total atoms	Number of unique orderings	Occupancy (cations per site)	Unique cation sites
Ca_3N_2	$Ia\bar{3}$	O	24/40	1	Ca: 1.0	48e
Zn_3N_2					Zn: 1.0	
Ca_3P_2	$P6_3/mcm$	D	9/15	2	Ca: 0.9	4d, 6g
Sr_3P_2	$I\bar{4}3d$		24/40	18	Sr: 1.0	16c
Zn_3P_2	$P4_2/nmc$*				Zn: 1.0	8g, 8g, 8g
$CaZn_2P_2$	$P\bar{3}m1$*	O	3/5	1	Ca: 1.0, Zn: 1.0	1a, 2d
$SrZn_2P_2$					Sr: 1.0, Zn: 1.0	
$ZnSr_2N_2$	$I4/mmm$*		6/10		Zn: 1.0, Ca: 1.0	2a, 4e
$ZnCa_2N_2$						
$ZnSr_2P_2$	$P6_3/mmc$	D	3/5		Zn: 0.5, Sr: 1.0	2a, 2d

structural and band gap information of all compounds considered are also compiled in Table S1 (ESI†). For the remaining compounds, we derived the initial configurations based on the available unique structures of other compounds (*i.e.*, unique space groups) *via* ionic substitution (see Section 3.1 for details). For structures that exhibited disorder within the cation and/or anion sublattices, we enumerated symmetrically distinct configurations using the OrderDisorderedStructureTransformation() class within pymatgen.[33] Note that the electronic structure, thermodynamic stability, and defect calculations were performed only for the ground state configuration (as evaluated by DFT) for each compound. To evaluate the thermodynamic stability, we calculated the 0 K convex hulls of the quaternary Ca–Sr–Zn–N and Ca–Sr–Zn–P systems, which includes the elements, and all possible binary, ternary, and quaternary ordered structures, as available in the ICSD.

To determine the dynamic stability and thermal properties of a select set of candidate pnictides, we performed phonon DOS calculations using the phonopy package[35] and the SCAN functional. We calculated the real-space force constants from 0.01 Å symmetrically distinct displacements of all atoms within each unit cell. For each atomic displacement, we performed a SCF calculation, with a total-energy convergence threshold of 10^{-6} eV that was sampled at the Γ point of the irreducible Brillouin zone. The resultant phonon frequencies and thermal properties were sampled on a $24 \times 24 \times 24$ mesh and the values are included in Fig. S12 and S13 of the ESI,† respectively. Note that negative frequencies in Fig. S12 (ESI†) correspond to imaginary phonon modes. The thermal properties in Fig. S13 (ESI†) are calculated ignoring any imaginary phonon modes and are normalized per formula unit for each composition.

For the five candidates, namely $ZnCa_2N_2$, $ZnSr_2N_2$, $SrZn_2N_2$, $CaZn_2P_2$, and $SrZn_2P_2$, we calculated the defect formation energies of cation vacancies, anion vacancies, and cation antisites. We used $3 \times 3 \times 2$ (90-atom) supercells of $CaZn_2P_2$, $SrZn_2P_2$, and $SrZn_2N_2$ and $3 \times 3 \times 2$ (180-atom) supercells of $ZnCa_2N_2$[12] and $ZnSr_2N_2$ to model the defective structures. The formation energy of any defect (E^f) is given by:[36]

$$E^f = E_{defect} - E_{bulk} - \sum_i n_i \mu_i + qE_F + E_{corr}$$

where E_{defect} and E_{bulk} are the total energies of supercell with and without defect, respectively, n_i represents the number of i-species atoms added (>0) and/or removed (<0) to form the defect with μ_i the corresponding chemical potential. We obtained the range of relevant μ_i for all vacancy defects considered from our 0 K convex hulls (values listed in Table S2 of ESI;† details of estimating μ ranges for each defect also provided in ESI†). The terms qE_F and E_{corr} indicate the exchange of

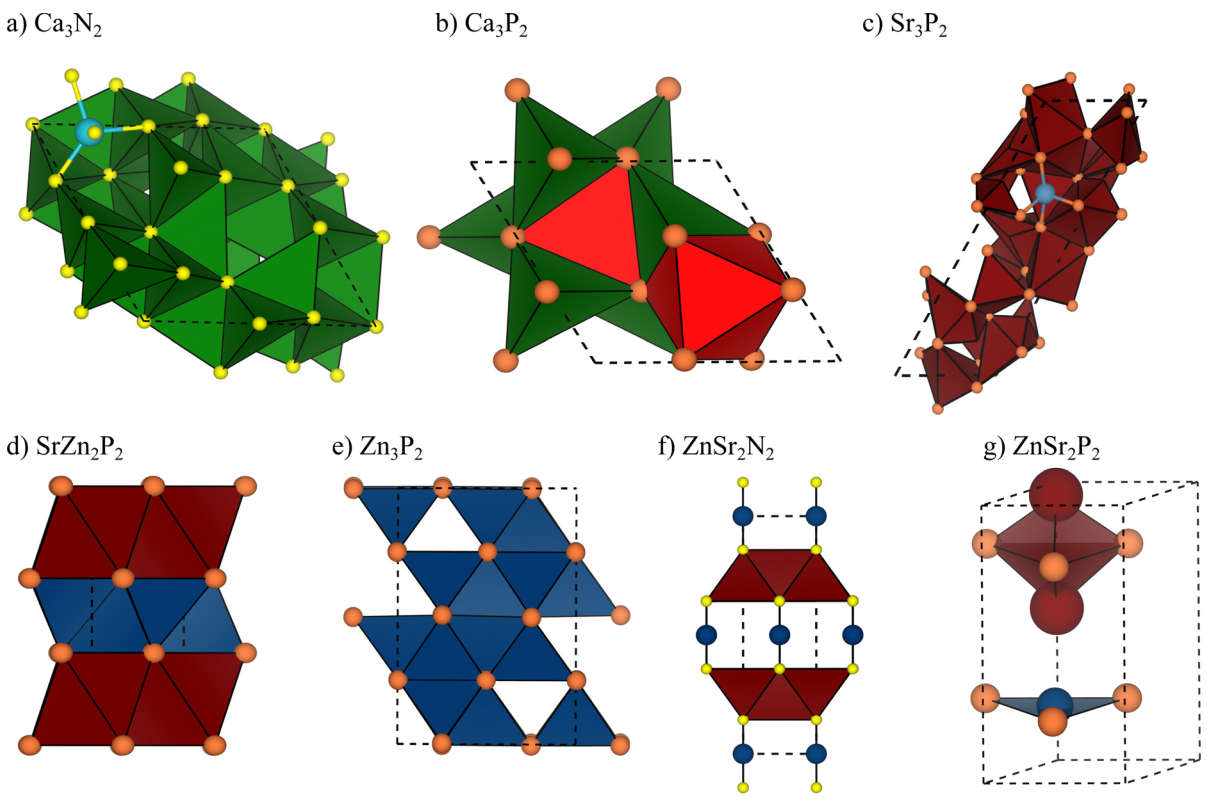

Fig. 1 Initial structures of nitrides and phosphides, as available in the ICSD, including (a) $Ia\bar{3}$-Ca_3N_2 (and Zn_3N_2), (b) $P6_3/mcm$-Ca_3P_2, (c) $I\bar{4}3d$-Sr_3P_2, (d) $P\bar{3}m1$-$SrZn_2P_2$ (and $CaZn_2P_2$), (e) $P4_2/nmc$-Zn_3P_2, (f) $I4/mmm$-$ZnSr_2N_2$ (and $ZnCa_2N_2$), and (g) $P6_3/mmc$-$ZnSr_2P_2$. The open polyhedron (panel a) shows the tetrahedral coordination of the Ca (or Sr) atom in Ca_3N_2 (in Sr_3P_2). Different shades of polyhedra in Ca_3P_2 (panel b) show the different coordination environments of tetrahedra (dark green) and octahedra (red) for Ca atom. Panels (d–f) are used as templates for generating other pnictide compositions. Color codes: Ca – green, Sr – brown, Zn – blue, N – yellow, and P – orange. In panels (d and f), Ca and Sr occupy identical sites in the corresponding Sr- and Ca-containing compounds.

charge(s) with the Fermi energy (E_F) of the pristine semiconductor and the corresponding correction term, which are relevant for the formation of charged defects. However, we have only considered neutral defects ($q = E_{corr} = 0$), which corresponds to removing (or adding) the entire atom to form a defect.

3 Results

3.1 Structures

Among the 20 pnictides considered in this work, the ICSD contains structures of 10 compounds, with the structural data compiled in Table 1 and the initial structures displayed in Fig. 1. The 10 compounds in Table 1 crystallize in six distinct space groups, namely anti-bixbyite $Ia\bar{3}$ (for Ca_3N_2 and Zn_3N_2, Fig. 1(a)), cubic $I\bar{4}3d$ (Sr_3P_2, Fig. 1(c)), tetragonal $P4_2/nmc$ (Zn_3P_2, Fig. 1(e)), tetragonal $I4/mmm$ ($ZnSr_2N_2$ and $ZnCa_2N_2$, Fig. 1(f)), hexagonal $P\bar{3}m1$ ($CaZn_2P_2$ and $SrZn_2P_2$, Fig. 1(d)), and hexagonal $P6_3/mmc$ (Ca_3P_2 of Fig. 1(b) and $ZnSr_2P_2$ of Fig. 1(g)).[12,37–42] For the disordered space groups in the ICSD, namely $Ia\bar{3}$, $P6_3/mmc$, and $I\bar{4}3d$ (see Table 1), we enumerate and obtain the symmetrically distinct orderings, with Fig. 1 displaying the lowest energy initial configurations for each space group. In the case of $I\bar{4}3d$-Sr_3P_2, we used a $3 \times 1 \times 1$ supercell for enumerating the disordered P sites, resulting in a 40-atom cell, while for other structures we used the unit cell for enumeration. For compounds whose structures are not available in the ICSD, we used the ordered structures with unique space groups in Table 1 (marked by "*" in the "space group" column) as templates and used chemical substitution and/or enumeration to derive the new initial structures. Details on the specific templating structures used with examples is provided in the ESI.† The DFT-calculated energies for the different initial configurations and the ground states (initial configurations) for all theory-derived structures are compiled in Tables S3, S4, and Fig. S2 of the ESI.†

3.2 Band gaps

All band gap (E_g) data, including the HSE06-calculated, SCAN-calculated, and available experimental values, are compiled in Table 2, which also lists whether the calculated DOS is originally from ICSD or a theoretical structure (see Section 3.1). In the case of $SrZn_2N_2$ and $CaZn_2N_2$, the E_g has been measured experimentally,[11,12] and the structures reported to be trigonal ($P\bar{3}m1$), in accordance with our results. However, the reported structures of $SrZn_2N_2$ and $CaZn_2N_2$ are not available in the ICSD, due to which we utilized our template + substitution strategy to obtain initial structures for our calculations. Notably, we find that all our SCAN-calculated E_g (in Table 2) are lower than HSE06-calculated E_g, which is expected since the inclusion of exact exchange in hybrid functionals facilitates electron localization and hence result in larger E_g than semi-local functionals (such as SCAN). There are also cases, namely Zn_3N_2 and $ZnSr_2P_2$, where SCAN predicts a qualitatively different (*i.e.*, metallic) electronic structure compared to HSE06, but such compounds may not be candidates for solar absorbers since their actual E_g may be low (*i.e.*, <1 eV).

Table 2 Band gaps (E_g in eV) of the pnictides considered in this work, as calculated using the SCAN and HSE06 functionals. Expt. indicates experimental data. The structural origin column indicates whether the initial structure was obtained from ICSD or *via* theoretical substitution of atoms. Space group of theoretical pnictides are based on the parent templates used

			E_g (eV)		
Compounds	Structural origin	Space group	SCAN	HSE06	Expt.
		Binaries			
Ca_3N_2	ICSD	$Ia\bar{3}$	1.19	1.75	1.90[15]
Ca_3P_2		$P6_3/mcm$	0.35	0.59	—
Sr_3N_2	Theoretical	$Ia\bar{3}$	0.40	0.93	—
Sr_3P_2		$I\bar{4}3d$	0.12	0.38	—
Zn_3N_2	ICSD	$Ia\bar{3}$	Metallic	0.64	1.23[43]
Zn_3P_2		$P4_2/nmc$	0.38	0.90	1.46[17]
		Ternaries			
$CaSr_2N_2$		$P4_2/nmc$	0.71	1.22	—
$CaSr_2P_2$	Theoretical		1.46	1.75	—
$SrZn_2N_2$			0.67	1.39	1.60[11]
$SrZn_2P_2$	ICSD		0.84	1.18	—
$CaZn_2N_2$	Theoretical	$P\bar{3}m1$	0.88	1.65	1.90[12]
$CaZn_2P_2$	ICSD		0.88	1.23	—
$SrCa_2N_2$	Theoretical		1.85	2.36	—
$SrCa_2P_2$			1.73	2.12	—
$ZnCa_2N_2$	ICSD		0.74	1.40	1.60[12]
$ZnCa_2P_2$	Theoretical	$I4/mmm$	0.36	0.80	—
$ZnSr_2N_2$	ICSD		0.89	1.38	—
$ZnSr_2P_2$		$P6_3/mmc$	Metallic	0.12	—
		Quaternaries			
$CaSrZnN_2$	Theoretical	$I4/mmm$	0.77	1.33	—
$CaSrZnP_2$		$P\bar{3}m1$	1.01	1.41	—

Interestingly, there are cases of nitrides exhibiting larger E_g than phosphides of the same cation composition (*e.g.*, Ca_3N_2 *vs.* Ca_3P_2, and $ZnCa_2N_2$ *vs.* $ZnCa_2P_2$), while the *vice versa* is also true in some cases (*e.g.*, Zn_3P_2 *vs.* Zn_3N_2, and $CaSr_2P_2$ *vs.* $CaSr_2N_2$). Importantly, the HSE06-E_g are in better agreement (but underestimating) with respect to the available experimental E_g than SCAN. The level of E_g underestimation by HSE06 is severe in binary pnictides (48% and 38% in Zn_3N_2 and Zn_3P_2, respectively), compared to the ternaries (13%, 13%, and 12.5% in $SrZn_2N_2$, $CaZn_2N_2$, and $ZnCa_2N_2$, respectively). Thus, for the selection of candidates with suitable band gaps for PV applications, we can still use the general range of 1.1–1.5 eV to ensure that there are no false negatives among the compositions considered.

Applying the 1.1–1.5 eV range within our HSE06-E_g, we find 6 possible ternary pnictides as candidate PVs, namely $CaSr_2N_2$ ($E_g \sim 1.22$ eV), $SrZn_2N_2$ (1.39 eV), $SrZn_2P_2$ (1.18 eV), $CaZn_2P_2$ (1.23 eV), $ZnCa_2N_2$ (1.40 eV), and $ZnSr_2N_2$ (1.38 eV), apart from the quaternaries, $CaSrZnN_2$ (1.33 eV) and $CaSrZnP_2$ (1.41 eV). Our calculated band gap in $ZnSr_2N_2$ (1.38 eV) is in agreement with a previous study utilizing the modified Becke–Johnson potential[44] ($\sim$1.45 eV[45]), although our predicted value for $ZnCa_2N_2$ (1.40 eV) is quite different from the same report ($\sim$1.72 eV[45]). Fig. 2 compiles the HSE06-calculated DOS for the six candidate ternaries, while the remaining HSE06 and

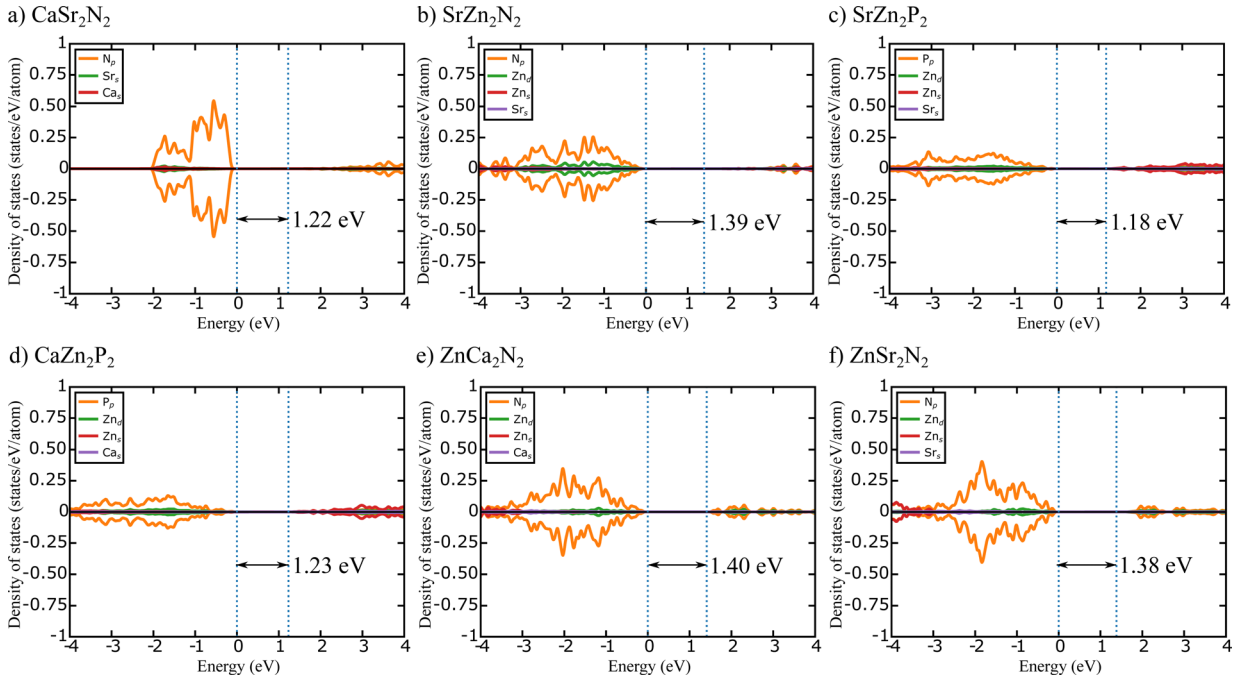

Fig. 2 HSE06-calculated DOS for the candidate pnictides. The density of states in each panel is normalized with respect to the total number of atoms within the calculated cell. Text annotation in each panel indicates the calculated band gap with the dotted blue lines highlighting the band edges.

SCAN-calculated DOS for all pnictides considered are displayed in the ESI† (Fig. S3–S9). The SCAN-calculated band structures for the six candidate pnictides are included in Fig. S10 (ESI†) and an examination of correlation between SCAN-calculated formation energies and band gaps is explored in Fig. S11 (ESI†). In all our DOS plots, the orange lines correspond to the anion (*i.e.*, N or P) p states, while the red, green, purple, and/or brown lines correspond to the cation s (for Ca, Sr, and Zn) and/or d (for Zn only) states. The dotted blue lines in our DOS panels indicate the valence and conduction band edges, while the Fermi level in metallic systems is displayed by dashed black lines. The zero on the energy scale in all DOS visualizations is set to the valence band maximum (VBM) in gapped systems, while the zero is set to the Fermi level in metallic systems.

Among the candidate ternaries, the VBM consists almost exclusively of the anionic p states, with low overlap of cationic s or d states, suggesting that the cation–anion bonds are quite ionic in nature. While anionic p states dominate the conduction band minimum (CBM) in $CaSr_2N_2$ (Fig. 2(a)), $ZnCa_2N_2$ (Fig. 2(e)) and $ZnSr_2N_2$ (Fig. 2(f)), the Zn s states do contribute significantly to the CBM in $SrZn_2N_2$ (Fig. 2(b)), $SrZn_2P_2$ (Fig. 2(c)), and $CaZn_2P_2$ (Fig. 2(d)). For ternary Zn-containing pnictides, we note that the HSE06-CBM is dominated by anionic p in nitrides, while Zn s states dominate CBM in phosphides, as illustrated by $SrZn_2N_2$ (Fig. 2(b))-$SrZn_2P_2$ (Fig. 2(c)), and $ZnSr_2N_2$ (Fig. 2(f)) and $ZnSr_2P_2$ (Fig. S8d, ESI†) pairs. However, for the $ZnCa_2N_2$ (Fig. 2(e)) and $ZnCa_2P_2$ (Fig. S8c, ESI†) pair, the anionic p dominates the CBM. Thus, cationic contributions to the CBM in ternaries, if any, only arise in Zn-containing compounds.

In the case of quaternaries, anionic p states dominates the VBM in both compounds, while N p and Zn s states dominate CBM in $CaSrZnN_2$ (Fig. S7f, ESI†) and $CaSrZnP_2$ (Fig. S9d, ESI†) respectively. Among the ternary candidates identified in our work, $SrZn_2N_2$, $ZnSr_2N_2$, and $ZnCa_2N_2$ have been explored as solar absorbers before (*i.e.*, E_g calculated and/or measured),[11,12] while the remaining compounds ($CaSr_2N_2$, $SrZn_2P_2$, and $CaZn_2P_2$) have not been studied as PVs so far. However, whether these compounds are feasible PV candidates depends on their thermodynamic stability (Section 3.3) and intrinsic tendency to form detrimental point defects (Section 3.4). Note that although the experimental band gaps of Zn_3N_2 and Zn_3P_2 are in the optimal range (1.23 eV and 1.46 eV, respectively), previous attempts at utilizing Zn_3P_2 as solar absorbers have yielded poor efficiencies, namely ~4% with expected Mg-doped improvements reaching 8–10% in Zn_3P_2.[46] Low efficiency in Zn_3P_2 have been attributed to difficulties in synthesizing p–n homojunctions of Zn_3P_2,[46] while the high moisture sensitivity and possible oxygen contamination of Zn_3N_2 has led to large variations in measured band gaps (1.06–3.2 eV),[47] with possible improvements in band gap engineering arising out of synthesizing $Zn_{3-3x}Mg_{3x}N_2$ alloys.[48] Hence, we will not be considering Zn_3N_2 and Zn_3P_2 as candidate materials in the rest of the manuscript.

3.3 Thermodynamic stability

We calculated the 0 K convex hulls for the quaternary systems, namely Ca–Sr–Zn–N and Ca–Sr–Zn–P, comprising of all the ordered structures available on ICSD and the theoretical/enumerated ground states that we have considered. For ease of

visualization, we have compiled three ternary projections for each quaternary system, namely, Ca–Sr–N, Ca–Zn–N, and Sr–Zn–N (panels a–c) for Ca–Sr–Zn–N quaternary, and Ca–Sr–P, Ca–Zn–P, and Sr–Zn–P (panels d–f) for Ca–Sr–Zn–P quaternary, in Fig. 3. All compounds that are stable at 0 K are indicated by green symbols in Fig. 3. Squares and circles in Fig. 3 indicate the non-candidate and the 20 candidate pnictides considered in this work. Note that previous theoretical studies have utilized a ~30 meV per atom energy above the hull (E^{hull}) threshold value,[49] beyond which synthesis of metastable/unstable compounds may become difficult experimentally. While we use 30 meV per atom as a stability threshold, we note that stability thresholds are often chemistry-dependent and a clear guideline for a threshold is not yet available for pnictides, given that several new compounds are being actively synthesized in this chemical space.[20]

We find all the ICSD-derived structures to be stable at 0 K, which is in line with expectations that the ICSD-derived structures have been experimentally characterized, with the only exception being $ZnSr_2P_2$ that is ~90 meV per atom unstable compared to other phases (Sr_3P_2 and $SrZn_2P_2$) in the Zn–Sr–P phase diagram (Fig. 3(f)). Note that the experimental structure of $ZnSr_2P_2$ is disordered, which typically results in an excess of configurational entropy that may stabilize the compound at higher temperatures, thus facilitating its synthesis. Among the theoretical structures, the stable pnictides are $SrZn_2N_2$, $CaZn_2N_2$, and $SrCa_2P_2$, out of which $SrZn_2N_2$ and $CaZn_2N_2$ have been reported to be synthesized before.[11,12] Thus, we find $SrCa_2P_2$ to be a stable compound that has not been experimentally reported nor theoretically studied in detail so far.

The unstable ternaries among the pnictides considered are, $CaSr_2N_2$ (E^{hull} ~ 72 meV per atom), $CaSr_2P_2$ (65 meV per atom), $SrCa_2N_2$ (34 meV per atom), and $ZnCa_2P_2$ (45 meV per atom) with the theoretical binary, Sr_3N_2 also marginally unstable (E^{hull} ~ 9 meV per atom). Both the theoretical quaternaries included in this work, $CaSrZnN_2$ and $CaSrZnP_2$ are also unstable (E^{hull} ~ 34 meV per atom and 68 meV per atom, respectively). Given the band gap data of Table 1 and Fig. 2, and including the 0 K thermodynamic stability as an additional filter, the set of viable PV candidates reduces to 5 compounds, $SrZn_2N_2$, $SrZn_2P_2$, $CaZn_2P_2$, $ZnCa_2N_2$, and $ZnSr_2N_2$, thus eliminating $CaSr_2N_2$ as a candidate due to its thermodynamic instability. Note that although metastable compounds (*e.g.*, $CaSrZnN_2$) may be synthesizeable, such compounds usually exhibit a higher tendency to form point defects than thermodynamically stable compounds.[50] Hence, for the calculation of point defect energies, we restrict ourselves to the above five candidates.

Notably, we have also evaluated the dynamic stability of the five candidates, by calculating the phonon DOS and the corresponding thermal properties, which are compiled in Fig. S12 and S13 (ESI†), respectively. With the exception of $ZnSr_2N_2$, we do not find any significant imaginary vibrational modes among the five identified candidates, with numerical noise contributing to minor non-zero imaginary modes (panels a–d in Fig. S12, ESI†). In the case of $ZnSr_2N_2$, the imaginary mode may have

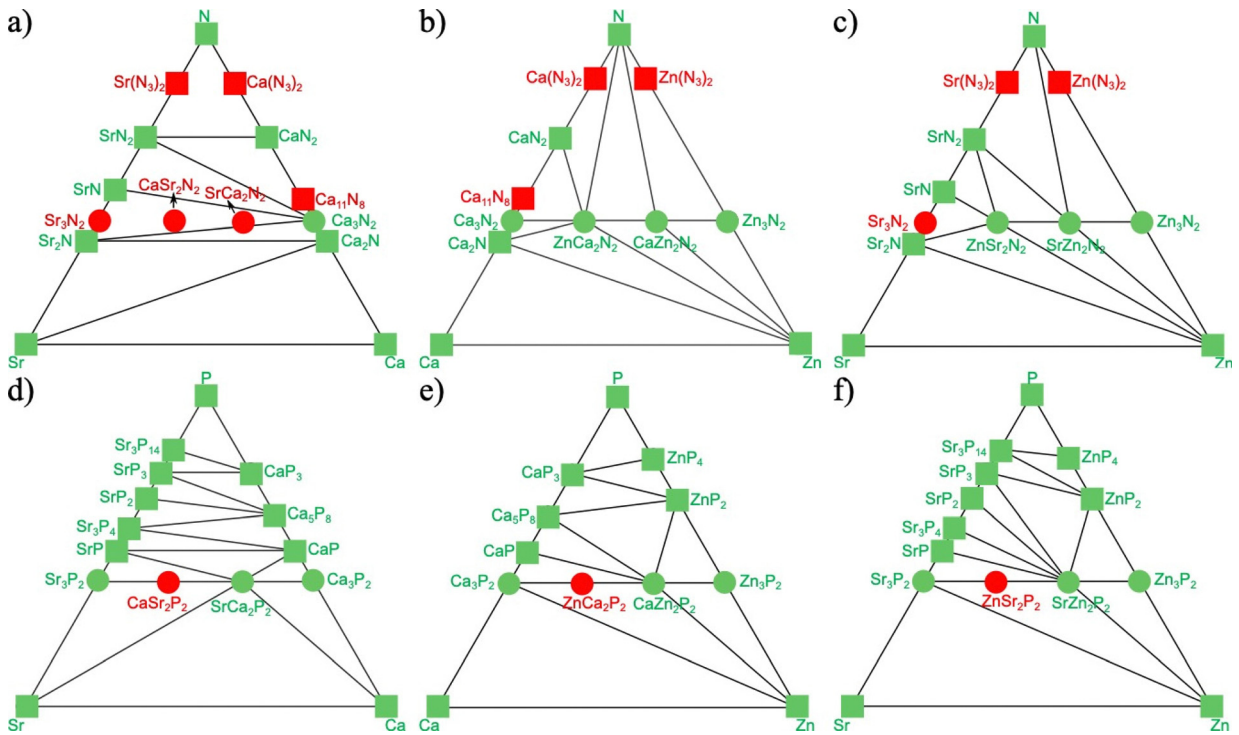

Fig. 3 SCAN-calculated 0 K ternary phase diagrams, including (a) Ca–Sr–N, (b) Ca–Zn–N, (c) Sr–Zn–N, (d) Ca–Sr–P, (e) Ca–Zn–P, and (f) Sr–Zn–P systems. Circles and squares correspond to candidate and non-candidate pnictides. Green and red symbols (and corresponding text annotations) are stable and unstable/metastable compounds, respectively.

been caused by the unit cell used in the phonon calculation, *i.e.*, we did not evaluate the phonon spectra within a supercell. Given that $ZnSr_2N_2$ is stable from our 0 K convex hull calculations (Fig. 3(c)) and is known to be experimentally synthesizable within the *I*4/*mmm* space group,[39] we do include $ZnSr_2N_2$ in the calculations of point defect energetics.

3.4 Point defect formation energies

For the five candidates identified from our band gap and stability calculations, namely, $SrZn_2N_2$, $SrZn_2P_2$, $CaZn_2P_2$, $ZnCa_2N_2$, and $ZnSr_2N_2$, we evaluate the point defect energetics, as displayed in Fig. 4. Specifically, we consider the formation of A and A′ cation vacancies (*i.e.*, Vac_A and $Vac_{A'}$ where Vac is vacancy, yellow and green bars in Fig. 4), anion vacancies (Vac_B, orange bar), and cation anti-site clusters ($A_{A'} + A'_A$, blue bar). For example, in the case of $SrZn_2N_2$, we calculate the energy of formation for Vac_{Sr}, Vac_{Zn}, Vac_N, and $Sr_{Zn} + Zn_{Sr}$ (*i.e.*, Sr occupying a Zn site + Zn occupying a Sr site). Hashed regions in Fig. 4 indicate the variation in the cation/anion vacancy formation energies with the corresponding change in the μ of the species being removed. The range of μ considered is based on the 0 K phase diagrams, *i.e.*, within the region of thermodynamic stability of the pnictide considered. In the case of anti-sites, we created a cluster by exchanging nearest possible neighbors of A and A′ atoms. The dashed black line in Fig. 4 indicates a 1 eV threshold of point defect formation energies. Although it is preferable for point defect formation energies to be as high as possible in pristine bulk phases, we use 1 eV as an arbitrary threshold to account for high-temperature synthesis protocols that may be used during fabrication. Additionally, point defects that exhibit formation energies that are above 1 eV have caused minimal performance deterioration in other candidate photovoltaics, such as kesterite-based chalcogenides.[3,50,51] Note that this 1 eV threshold can be changed, if necessary.

Importantly, we find that all the five candidates exhibit anti-site cluster and cation vacancy formation energies well above the 1 eV threshold (Fig. 4), ranging from $\sim$1.42 eV for Vac_{Ca} in $CaZn_2P_2$ to 5.25 eV for Vac_{Ca} in $ZnCa_2N_2$, highlighting the large degree of resistance that the candidate pnictides exhibit for formation of such defects. In terms of anion vacancies, while $SrZn_2N_2$ (2.29–2.64 eV), $SrZn_2P_2$ (2.02–3.26 eV), and $CaZn_2P_2$ (1.88–3.17 eV) exhibit formation energies above the 1 eV threshold, $ZnCa_2N_2$ (0.42–2.14 eV) and $ZnSr_2N_2$ (0.47–2.00 eV) do not, indicating that the former three compounds exhibit better resistance to n-type anion vacancies, especially under anion-poor conditions. Thus, combining the band gap, thermodynamic stability, and high degree of resistance to point defect energetics, we find $SrZn_2N_2$, $SrZn_2P_2$, and $CaZn_2P_2$ to be the most promising candidate materials for PV applications. In case low temperature synthesis and/or heat treatment protocols are utilized, we believe that $ZnCa_2N_2$ and $ZnSr_2N_2$ may also be relevant for PVs, since their defect formation energies are higher than the values reported for common point defects in kesterite-based PV materials.[3,29,52,53] While $SrZn_2N_2$ has been explored for its semiconducting properties before,[11] $SrZn_2P_2$ and $CaZn_2P_2$ are novel candidates whose electronic properties have not been explored *a priori*.

4 Discussion

Using DFT calculations, we have explored the binary, ternary, and quaternary divalent-metal-based pnictide chemical space as candidate beyond-Si photovoltaic materials in this work.

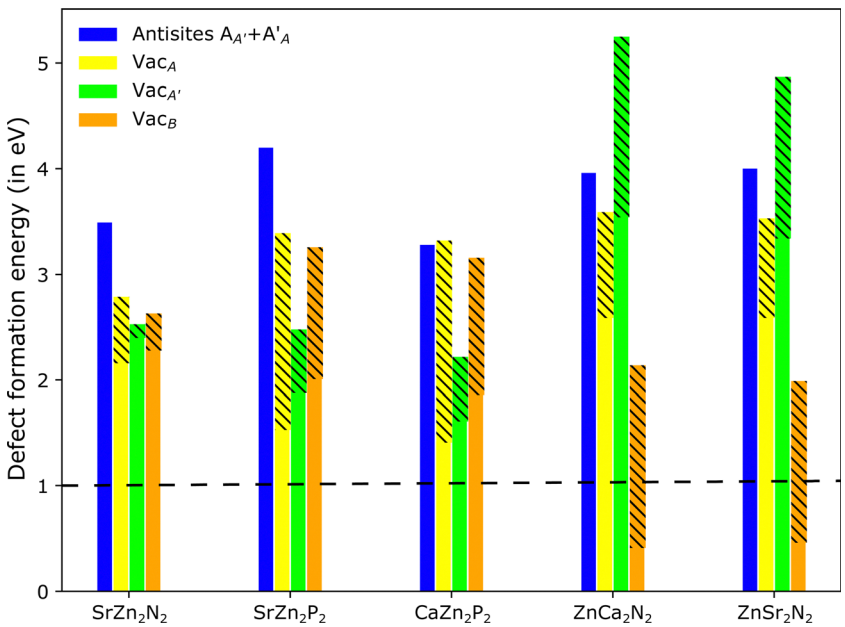

Fig. 4 Point defect formation energies for A-site and A′-site cation vacancies (Vac_A and $Vac_{A'}$, yellow and green bars), anion vacancies (Vac_B), and cation anti-site clusters ($A_{A'} + A'_A$). The ternaries considered exhibit a composition of AA'_2B_2. Hashed regions signify variation in vacancy formation energies with change in the chemical potential of the species removed.

Specifically, we considered a set a twenty compounds, comprising A_3B_2 binaries, AA'_2B_2 ternaries, and $AA'A''B_2$ quaternaries (A, A′, A″ = Ca, Sr, or Zn; B = N or P) and quantified their ground state configurations, band gaps, 0 K thermodynamic stability, dynamic stability *via* phonon calculations, and formation energies of select point defects. Importantly, we identified $SrZn_2N_2$, $SrZn_2P_2$, and $CaZn_2P_2$ as candidate materials based on the properties calculated, besides $ZnCa_2N_2$ and $ZnSr_2N_2$, which are susceptible to Vac_N formation.

For the pnictides whose structures were unavailable in the ICSD, we calculated the ground state configuration by considering possible structures using other binary and ternary pnictide unit cells that were available as templates. However, we did not consider the possibility of cation arrangements forming superlattices over larger distances, which requires the consideration of larger supercells (instead of smaller unit cells), thus significantly increasing computational costs. Thus, for the candidate ternaries that we have identified (namely, $SrZn_2N_2$, $SrZn_2P_2$, and $CaZn_2P_2$), it may be useful to explore the possibility of superlattice formation. Also, we did not consider the anti-bixbyite structure of Ca_3N_2/Zn_3N_2 as templates for the ternary and quaternary structures since the structure has 48 symmetrically distinct cation sites and decorating, say, 16 sites each of Ca, Sr, and Zn is computationally intractable. Hence, we do not rule out our candidate ternaries from crystallizing in anti-bixbyite-based structures.

We carried out DOS calculations using SCAN and HSE06 because the former typically underestimates E_g. Since hybrid functionals include a portion of the exact exchange, their band gap estimates are typically better due to the consequent reduction in self-interaction errors compared to semi-local functionals. Indeed, previous studies have reported better agreement in band gap estimates with HSE06 *vs.* experiments compared to SCAN in kesterite photovoltaics.[30,50] However, hybrid functionals do not guarantee the best theoretical estimates of E_g, which typically require quasi-particle calculations, such as the single-shot GW calculation (*i.e.*, G_0W_0), which have shown excellent agreement with experimental photoemission spectroscopy/inverse photoemission spectroscopy measurements before.[54,55] However, the computational costs of GW calculations are even higher than hybrid functionals, which is the reason we did not pursue such calculations for all the twenty compounds considered in our work.

The synthesis of nitrides is difficult given their tendency to decompose at higher temperatures due to lower formation energies (compared to oxides),[12] the strong triple bond of N_2 molecule, and stringent conditions of oxygen and water-free conditions to achieve high purity.[56,57] Hence, we have focused solely on compounds that are stable at 0 K since we expect the synthesis to be easier compared to metastable compounds ($E^{hull} \leq 30$ meV per atom), which may require higher temperatures and/or pressures. So far, synthesis of Ca and Zn based ternary nitrides have been performed *via* solid state techniques, using binary Ca_3N_2 and Zn_3N_2 as precursors,[12] where $ZnCa_2N_2$ required Ar-atmosphere and $CaZn_2N_2$ needed high pressure and an elevated temperature.[12] Besides synthesis difficulties, the air and moisture sensitivity of the candidate compounds (both nitrides and phosphides), particularly during operation as a photovoltaic, and the consequent impact on solar absorption efficiencies remains to be quantified. In the case of phosphides, the possible formation of the highly-toxic phosphine gas, either during synthesis or during operation, is also a concern.[58,59] Another challenge with pnictides will be the ability to form p–n homojunctions, instead of relying on other materials to form heterojunction-based devices.[46]

While DFT often does not provide quantitative accuracy for defect formation energies, previous studies have shown that SCAN can provide an upper bound (compared to other semi-local functionals) on defect formation energies, with qualitative trends being similar across different functionals for a given compound.[30,36] For reducing quantitative error in defect formation energies, we need further improvements in the XC functional and likely shoulder higher computational costs. Nevertheless, we expect all candidate pnictides shown in Fig. 4 to be significantly more resistant to point defect formation, such as cation vacancies, cation anti-sites, and anion vacancies, compared to other compound semiconductors, such as Cu_2ZnSnS_4.

5 Conclusion

The design of new semiconducting beyond-Si materials that can achieve reasonable solar-to-electricity conversion efficiencies, and that consist of relatively abundant and non-toxic elements is a key ingredient in moving towards non-fossil-fuel-based sources of energy. In this work, we have used DFT calculations to systematically explore the pnictide chemical space, including binary A_3B_2, ternary AA'_2B_2, and quaternary $AA'A''B_2$ compounds, where A, A′, and A″ are non-redox-active divalent cations (namely Ca, Sr, or Zn), and B is either N or P. In total, we considered a set of 20 pnictide compositions, out of which 10 were experimentally known structures and we created the initial (theoretical) structures of the remaining 10 compounds using experimentally-available template structures. Upon identifying the DFT-calculated ground state configurations of all 20 compositions, we evaluated the band gaps, 0 K thermodynamic and dynamic stability, and the resistance to formation of cation/anion vacancies and cation anti-sites. For treating the electronic exchange and correlation, we used a combination of the SCAN and HSE06 functionals, with SCAN used for structure relaxations and HSE06 for band gap evaluations. Wherever possible, we benchmarked our calculated values with those available in the literature. Importantly, we found a set of five pnictide compositions that exhibit HSE06-calculated band gaps in the optimal (1.1–1.5 eV) range, are thermodynamically stable at 0 K, and are resistant to formation of point defects (formation energy >0.4 eV), namely, $SrZn_2N_2$, $SrZn_2P_2$, $CaZn_2P_2$, $ZnCa_2N_2$, and $ZnSr_2N_2$. Among the candidates identified, we found $SrZn_2N_2$, $SrZn_2P_2$, and $CaZn_2P_2$ to be particularly resistant to forming point defects (formation energies >1 eV), while the other compounds ($ZnCa_2N_2$ and $ZnSr_2N_2$) are

susceptible to Vac_N formation (0.42–0.47 eV). We hope that our study will ignite further interest in the pnictide chemical space and enable the practical realization of some of the candidates identified in this work as beyond-Si photovoltaics.

Data availability

All the computational data presented in this study are freely available to all on our GitHub repository (**https://github.com/sai-mat-group/pv-nitrides**).

Conflicts of interest

There are no conflicts to declare.

Acknowledgements

G. S. G acknowledges financial support from the Indian Institute of Science (IISc) Seed Grant, SG/MHRD/20/0020 and SR/MHRD/20/0013. J. K. thanks the Ministry of Human Resource Development, Government of India, for financial assistance. The authors acknowledge the computational resources provided by the Supercomputer Education and Research Centre, IISc, for enabling some of the density functional theory calculations showcased in this work.

References

1 **www.futureforall.org/energy/solar_energy.htm**.
2 W. Shockley and H. J. Queisser, Detailed Balance Limit of Efficiency of p–n Junction Solar Cells, *J. App. Phys.*, 2015, 510.
3 G. S. Gautam, T. P. Senftle and E. A. Carter, Understanding the Effects of Cd and Ag Doping in Cu_2ZnSnS_4 Solar Cells, *Chem. Mater.*, 2018, **30**, 4543–4555.
4 T. D. Lee and A. U. Ebong, A review of thin film solar cell technologies and challenges, *Renewable Sustainable Energy Rev.*, 2017, **70**, 1286–1297.
5 T. Feurer, P. Reinhard, E. Avancini, B. Bissig, J. Löckinger and P. Fuchs, *et al.*, Progress in thin film CIGS photovoltaics – Research and development, manufacturing, and applications, *Prog. Photovoltaics Res. Appl.*, 2017, **25**(7), 645–667.
6 S. Sharma, K. K. Jain and A. Sharma, Solar Cells: In Research and Applications—A Review, *Mater. Sci. Appl.*, 2015, **06**(12), 1145–1155.
7 , Editorial, Elements in short supply, *Nat Mater.*, 2011, **10**(3), 157.
8 L. Chen, S. Soltanmohammad, J. W. Lee, B. E. McCandless and W. N. Shafarman, Secondary phase formation in (Ag,Cu)(In,Ga)Se_2 thin films grown by three-stage co-evaporation, *Sol. Energy Mater. Sol. Cells*, 2017, **166**, 18–26.
9 P. Hohenberg and W. Kohn, Inhomogeneous electron gas, *Phys. Rev.*, 1964, **136**, B864–B871.
10 W. Kohn and L. J. Sham, Self-consistent equations including exchange and correlation effects, *Phys. Rev.*, 1965, **140**, A1133–A1138.
11 R. Kikuchi, K. Ueno, T. Nakamura, T. Kurabuchi, Y. Kaneko and Y. Kumagai, *et al.*, $SrZn_2N_2$ as a Solar Absorber: Theoretical Defect Chemistry and Synthesis by Metal Alloy Nitridation, *Chem. Mater.*, 2021, **33**(8), 2864–2870.
12 Y. Hinuma, T. Hatakeyama, Y. Kumagai, L. A. Burton, H. Sato and Y. Muraba, *et al.*, Discovery of earth-abundant nitride semiconductors by computational screening and high-pressure synthesis, *Nat. Commun.*, 2016, 1–2.
13 M. Tsuji, H. Hiramatsu and H. Hosono, Tunable Light Emission through the Range 1.8–3.2 eV and p-Type Conductivity at Room Temperature for Nitride Semiconductors, $Ca(Mg(1-x)Zn(x))_2N_2$ (x = 0–1), *Inorg. Chem.*, 2019, **58**(18), 12311–12316.
14 G. Murtaza, A. A. Khan, M. M. AL-Anazy, A. Laref, Q. Mahmood and Z. Zada, *et al.*, Anionic variations for $BaMg_2X_2$ (X = N to Bi) compounds by density functional theory, *Eur. Phys. J. Plus*, 2021, **136**(2), 1–16.
15 E. Orhan, S. Jobic, R. Brec, R. Marchand and J. Saillard, Binary nitrides α-M_3N_2 (M – Be, Mg, Ca): a theoretical study, *J. Mater. Chem.*, 2002, **2**, 2475–2479.
16 J. M. Pawlikowski, J. Misiewicz and N. Mirowska, Direct and indirect optical transitions in Zn_3P_2, *J. Phys. Chem. Solids*, 1979, **40**, 1027–1033.
17 J. M. Pawlikowski, Optical band gap of Cd_3P_2–Zn_3P_2 semiconductor solid solutions, *J. Phys. C*, 1985, **18**, 5605–5616.
18 R. Long, Y. Dai, L. Yu, B. Huang and S. Han, Atomic geometry and electronic structure of defects in Zn_3N_2, *Thin Solid Films*, 2008, **516**, 1297–1301.
19 A. L. Greenaway, C. L. Melamed, M. B. Tellekamp, R. Woods-Robinson, E. S. Toberer and J. R. Neilson, *et al.*, Ternary Nitride Materials: Fundamentals and Emerging Device Applications, *Annu. Rev. Mater. Res.*, 2021, **51**, 591–618.
20 W. Sun, C. J. Bartel, E. Arca, S. R. Bauers, B. Matthews and B. Orvañanos, *et al.*, A map of the inorganic ternary metal nitrides, *Nat. Mater.*, 2019, **18**(7), 732–739.
21 G. Kresse and J. Hafner, Ab initio molecular dynamics for liquid metals, *Phys. Rev. B: Condens. Matter Mater. Phys.*, 1993, **47**(1), 558–561.
22 G. Kresse and J. Furthmu, Efficient iterative schemes for ab initio total-energy calculations using a plane-wave basis set, *Phys. Rev. B: Condens. Matter Mater. Phys.*, 1996, **54**(16), 11169.
23 G. Kresse and D. Joubert, From ultrasoft pseudopotentials to the projector augmented-wave method, *Phys. Rev. B: Condens. Matter Mater. Phys.*, 1999, **59**(3), 11–19.
24 H. J. Monkhorst and J. D. Pack, Special points for Brillouin-zone integrations, *Phys. Rev. B: Solid State*, 1976, **13**, 5188–5192.
25 J. Sun, A. Ruzsinszky and J. P. Perdew, Strongly Constrained and Appropriately Normed Semilocal Density Functional, *Phys. Rev. Lett.*, 2015, **036402**, 1–6.
26 G. Sai Gautam and E. A. Carter, Evaluating transition metal oxides within DFT-SCAN and SCAN+*U* frameworks for solar thermochemical applications, *Phys. Rev. Mater.*, 2018, **2**(9), 1–14.

27 O. Y. Long, G. Sai Gautam and E. A. Carter, Evaluating optimal U for 3d transition-metal oxides within the SCAN+*U* framework, *Phys. Rev. Mater.*, 2020, **4**(4), 1–15.
28 O. Y. Long, G. Sai Gautam and E. A. Carter, Assessing cathode property prediction: *Via* exchange–correlation functionals with and without long-range dispersion corrections, *Phys. Chem. Chem. Phys.*, 2021, **23**(43), 24726–24737.
29 S. Berman, G. Sai Gautam and E. A. Carter, Role of Na and Ca as Isovalent Dopants in Cu_2ZnSnS_4 Solar Cells., *ACS Sustain Chem. Eng.*, 2019, **7**(6), 5792–5800.
30 R. B. Wexler, G. S. Gautam and E. A. Carter, Exchange–correlation functional challenges in modeling quaternary chalcogenides, *Phys. Rev. B*, 2020, **102**(5), 54101.
31 J. Heyd, G. E. Scuseria and M. Ernzerhof, Hybrid functionals based on a screened Coulomb potential, *J. Chem. Phys.*, 2003, **118**(18), 8207–8215.
32 W. Setyawan and S. Curtarolo, High-throughput electronic band structure calculations: Challenges and tools, *Comput. Mater. Sci.*, 2010, **49**(2), 299–312.
33 S. Ping, W. Davidson, A. Jain, G. Hautier, M. Kocher and S. Cholia, *et al.*, Python Materials Genomics (pymatgen): A robust, open-source python library for materials analysis, *Comput. Mater. Sci.*, 2013, **68**, 314–319.
34 M. Hellenbrandt, The inorganic crystal structure database (ICSD) - Present and future, *Crystallogr. Rev.*, 2004, **10**(1), 17–22.
35 A. Togo and I. Tanaka, First principles phonon calculations in materials science, *Scr. Mater.*, 2015, **108**, 1–5.
36 C. Freysoldt, B. Grabowski, T. Hickel, J. Neugebauer, G. Kresse and A. Janotti, *et al.*, First-principles calculations for point defects in solids, *Rev. Mod. Phys.*, 2014, **86**, 253–305.
37 A. M. Heyns, L. C. Prinsloo and M. Stassen, The Vibrational Spectra and Decomposition of Calcium Nitride (Ca_3N_2) and Magnesium Nitride (Mg_3N_2), *J. Solid State Chem.*, 1998, **41**(137), 33–41.
38 I. E. Zanin, K. B. Aleinikova, M. M. Afanasiev and M. Y. Antipin, Structure of Zn_3P_2, *J. Struct. Chem.*, 2004, **45**(5), 844–848.
39 H. Yamane and F. J. Disalvo, Synthesis and Crystal Structure of Sr_2ZnN_2 and Ba_2ZnN_2, *J. Solid State Chem.*, 1995, **379**, 375–379.
40 P. Klufers and A. Mewis, AB_2X_2 Compounds with the $CaAl_2Si_2$ Structure, II1 (A = Ca; B = Zn, Cd; X = P, As), *Z. Naturforsch.*, 1977, **32**, 353–354.
41 L. S. Xie, L. M. Schoop and E. M. Seibel, A new form of Ca_3P_2 with a ring of Dirac nodes, *APL Mater.*, 2015, **3**, 083602.
42 D. K. Wilson, B. Saparov and S. Bobev, Synthesis, Crystal Structures and Properties of the Zintl Phases Sr_2ZnP_2, Sr_2ZnAs_2, A_2ZnSb_2 and A_2ZnBi_2 (A = Sr and Eu), *J. Inorg. Gen. Chem.*, 2018, **2**, 2018–2025.
43 F. Zong, H. Ma, C. Xue, H. Zhuang and X. Zhang, Synthesis and thermal stability of Zn_3N_2 powder, *Solid State Commun.*, 2004, **132**, 521–525.
44 F. Tran and P. Blaha, Accurate band gaps of semiconductors and insulators with a semilocal exchange–correlation potential, *Phys. Rev. Lett.*, 2009, **102**(22), 5–8.
45 G. K. Balci and S. S. Ayhan, The first principle study: Structural, electronic and optical properties of X_2ZnN_2 (X: Ca, Ba, Sr), *J Non-Oxide Glasses*, 2019, **11**(1), 9–18.
46 G. M. Kimball, N. S. Lewis and H. A. Atwater, Mg doping and alloying in Zn_3P_2 heterojunction solar cells, *Conf. Rec. IEEE Photovoltaic Spec. Conf.*, 2010, 1039–1043.
47 T. Suda and K. Kakishita, Band-gap energy and electron effective mass of polycrystalline Zn_3N_2, *J. Appl. Phys.*, 2006, **99**(7), 1–4.
48 P. Wu, X. Cao, T. Tiedje and N. Yamada, Bandgap tunable $Zn_{3-3x}Mg_{3x}N_2$ alloy for earth-abundant solar absorber, *Mater. Lett.*, 2019, **236**, 649–652.
49 W. Lu, J. Wang, G. Sai Gautam and P. Canepa, Searching Ternary Oxides and Chalcogenides as Positive Electrodes for Calcium Batteries, *Chem. Mater.*, 2021, **33**(14), 5809–5821.
50 G. S. Gautam, R. B. Wexler and E. A. Carter, Optimizing kesterite solar cells from Cu_2ZnSnS_4 to $Cu_2CdGe(S,Se)_4$, *J. Mater. Chem.*, 2021, **39**, 9882–9897.
51 S. Hadke, S. Levcenko, G. Sai Gautam, C. J. Hages, J. A. Márquez and V. Izquierdo-Roca, *et al.*, Suppressed Deep Traps and Bandgap Fluctuations in Cu_2CdSnS_4 Solar Cells with ≈8% Efficiency, *Adv. Energy Mater.*, 2019, **9**(45), 1–11.
52 S. Chen, J. Yang and X. G. Gong, Intrinsic point defects and complexes in the quaternary kesterite semiconductor Cu_2ZnSnS_4, *Phys. Rev. B: Condens. Matter Mater. Phys.*, 2010, 35–37.
53 S. Chen, A. Walsh, X. G. Gong and S. H. Wei, Classification of lattice defects in the kesterite Cu_2ZnSnS_4 and $Cu_2ZnSnSe_4$ earth-abundant solar cell absorbers, *Adv. Mater.*, 2013, **25**(11), 1522–1539.
54 N. Alidoust, M. Lessio and E. A. Carter, Cobalt(II) oxide and nickel(II) oxide alloys as potential intermediate-band semiconductors: A theoretical study, *J. Appl. Phys.*, 2016, **119**(2), 025102.
55 N. Alidoust, M. C. Toroker, J. A. Keith and E. A. Carter, Significant reduction in NiO band gap upon formation of $Li_xNi_{1-x}O$ alloys: Applications to solar energy conversion, *ChemSusChem*, 2014, **7**(1), 195–201.
56 S. H. Elder and F. J. DiSalvo, Thermodynamics of Ternary Nitride Formation by Ammonolysis: Application to $LiMoN_2$, Na_3WN_3, and Na_3WO_3N, *Chem Mater.*, 1993, **22**, 1545–1553.
57 J. M. McHale, A. Navrotsky, G. R. Kowach, V. E. Balbarin and F. J. Disalvo, Energetics of Ternary Nitrides: Li–Ca–Zn–N and Ca–Ta–N Systems, *Chem. Mater.*, 1997, **9**(7), 1538–1546.
58 R. Rothfelder, V. Streitferdt, U. Lennert, J. Cammarata, D. J. Scott and K. Zeitler, *et al.*, Photocatalytic Arylation of P_4 and PH_3: Reaction Development Through Mechanistic Insight, *Angew. Chem., Int. Ed.*, 2021, **60**(46), 24650–24658.
59 K. Kakishita, S. Ikeda and T. Suda, Zn_3P_2 epitaxial growth by MOCVD, *J. Cryst. Growth*, 1991, **115**(1–4), 793–797.